An Investigation of Extreme Cold Events at the South Pole

LINDA M. KELLER,[a] KATHRYN J. MALONEY,[a] MATTHEW A. LAZZARA,[a,b] DAVID E. MIKOLAJCZYK,[a] AND STEFANO DI BATTISTA[c]

[a] *Antarctic Meteorological Research Center, Space Science and Engineering Center, University of Wisconsin–Madison, Madison, Wisconsin*
[b] *Department of Physical Sciences, School of Engineering, Science, and Mathematics, Madison Area Technical College, Madison, Wisconsin*
[c] *Meteogiornale, Milan, Italy*

(Manuscript received 21 May 2021, in final form 11 December 2021)

ABSTRACT: From 5 July to 11 September 2012, the Amundsen–Scott South Pole station experienced an unprecedented 78 days in a row with a maximum temperature at or below −50°C. Aircraft and ground-based activity cannot function without risk below this temperature. Lengthy periods of extreme cold temperatures are characterized by a drop in pressure of around 15 hPa over 4 days, accompanied by winds from grid east. Periodic influxes of warm air from the Weddell Sea raise the temperature as the wind shifts to grid north. The end of the event occurs when the temperature increase is enough to move past the −50°C threshold. This study also examines the length of extreme cold periods. The number of days below −50°C in early winter has been decreasing since 1999, and this trend is statistically significant at the 5% level. Late winter shows an increase in the number of days below −50°C for the same period, but this trend is not statistically significant. Changes in the southern annular mode, El Niño–Southern Oscillation, and the interdecadal Pacific oscillation/tripole index are investigated in relation to the initiation of extreme cold events. None of the correlations are statistically significant. A positive southern annular mode and a La Niña event or a central Pacific El Niño–Southern Oscillation pattern would position the upper-level circulation to favor a strong, symmetrical polar vortex with strong westerlies over the Southern Ocean, leading to a cold pattern over the South Pole.

SIGNIFICANCE STATEMENT: The Amundsen–Scott South Pole station is the coldest Antarctic station staffed year-round by U.S. personnel. Access to the station is primarily by airplane, especially during the winter months. Ambient temperature limits air access as planes cannot operate at minimum temperatures below −50°C. The station gets supplies during the winter months if needed, and medical emergencies can happen requiring evacuations. Knowing when planes would be able to fly is crucial, especially for life-saving efforts. During 2012, a record 78 continuous days of temperatures below −50°C occurred. A positive southern annular mode denoting strong westerly winds over the Pacific Ocean and a strong polar vortex over the South Pole contribute to the maintenance of long periods of extremely cold temperatures.

KEYWORDS: Atmosphere; Antarctica; Climatology; Climate records; Climate variability

1. Introduction

The U.S. Meteorological Station Amundsen–Scott was established at the geographic South Pole, 2836 m above mean sea level (MSL), in November 1956. The routine observations began on 9 January 1957 (11 January for temperature values) with no breaks in the record to the present time. At the beginning, the extremes of the Antarctic climate on the Polar Plateau were unknown. The U.S. Weather Bureau tried to calculate the possible minimum temperature near the ground at the South Pole in virtually optimum circumstances, i.e., simultaneous absence of solar radiation, clear skies, and calm wind for the entire polar night. The result of this quantitative analysis was that after 180 days, the snow surface temperature dropped to around −200°C (McCormick 1958). The scientific leader of the station based his prediction of −120°F (−84.4°C) for the average of the coldest month of winter, 1957 on this erroneous theory (Siple 1957; Siple 1959; Wendler and Kodama 1993). In the first operational year, the station recorded a daily minimum of −74.4°C, and the first value lower than −80°C was observed after 9 years of station operation on 21 July 1965 (−80.6°C). The absolute minimum was recorded on 23 June 1982 (−82.8°C). [Turner et al. (2021) reports −81.7°C, but that is based on synoptic reporting times, not the absolute minimum for the day.] The last reported value lower than −80°C was recorded on 14 September 1997 (−80.4°C). The maximum was reached on 25 December 2011 (−12.3°C). The annual mean temperature for the period 1957–2020 is −49.3°C. The area is known for strong surface temperature inversions as large as 20°–25°C in the winter (Connolley 1996). Differences between early and late winter in temperature, pressure, and wind speed (van Loon 1967; van den Broeke 1998a; Lazzara et al. 2012) support separation into five seasons: summer (December–January), autumn (February–March), early winter (April–June), late winter (July–September),

Denotes content that is immediately available upon publication as open access.

Corresponding author: Linda M. Keller, lmkeller@wisc.edu

DOI: 10.1175/JCLI-D-21-0404.1

and spring (October–November) (see Fig. 1 from Lazzara et al. 2012).

The persistence of cold temperatures for lengthy periods of time is important because access to the station is primarily by aircraft. The cold creates logistical challenges for aircraft and ground-based aircraft operations. The limits for acceptable risk are −50°C on the ground, −55°C in flight, −54°C for the hydraulics, and −58°C for the fuel (Lazzara et al. 2012). A description of the difficulties of operation for a winter medevac is given in Monaghan et al. (2003). The record-breaking persistence of cold temperatures in 2012 (lasting from 5 July to 20 September) inspired this study. During this time, the temperature at 2 m remained at or below −50°C for 78 consecutive days.

The paper is organized as follows: section 2 describes the data and climate indices that were used; section 3 discusses the characteristics of the cold events and the changes over time, as well as the possible influences of the changing climate regimes in the South Pacific; and section 4 contains the discussion of the results and the conclusions.

2. Data/methodology

Extreme cold periods were defined as a series of 20 or more consecutive days with a maximum near-surface temperature at or below −50°C. Amundsen–Scott South Pole station data from 1957 to 2020 were obtained from the Antarctic Meteorological Research Center's (AMRC) Data Server archives. [See Lazzara et al. (2012) for a detailed station history, any data corrections made by the AMRC prior to archiving, and a 50-yr climatology of the station.] For this study, the accuracy of the temperature instrument was considered (Keller et al. 2009). The temperature instruments had an accuracy of 0.3°C, so the maximum temperature allowed for the event was adjusted to −49.7°C. The result of this adjustment was to lengthen some events by 1–13 days (10 events) or add an event that was originally less than 20 days in duration (8 new events). The FMQ-19 temperature sensor with an accuracy of 0.1°C was installed in 2005 (Lazzara et al. 2012), and the adjustment was no longer needed. The length of the longest extreme cold event annually, the number of extreme cold events lasting 20+ days and 40+ days annually, the number of cold event days annually, and the months during which each cold event occurred were recorded. Additionally, the number of winter days below −50°C spanning 1957–2020 was calculated using archived data. Average pressure during these periods for events lasting 20+ days was also recorded.

Climate indices were examined to judge the influence of the patterns they describe on the change in temperature and wind direction. Monthly southern annular mode (SAM) indices were obtained from the observations and reanalyses of Dr. Gareth Marshall of the British Antarctic Survey (Marshall 2003, 2022) and describe the strength of the westerlies. The oceanic Niño index (ONI) was used to define the occurrence of El Niño or La Niña (greater than +0.5 or less than −0.5, respectively) (Huang et al. 2017; NOAA/NWS/Climate Prediction Center 2022). After the identification of an El Niño–Southern Oscillation (ENSO) event, the strength of the anomaly in the Niño-3 and Niño-4 areas was used to assign the position of the SST anomaly to the eastern or central Pacific (Rayner et al. 2003; NOAA/Physical Sciences Laboratory 2022a). The position of the Pacific–South America (PSA) pattern, a Rossby wave train generated by tropical heating anomalies (Ashok et al. 2007, 2009; Wilson et al. 2014; Lachlan-Cope and Connolley 2006), was also examined. The PSA pattern is represented by the second and third empirical orthogonal functions (EOFs) of the 500-hPa height anomalies and is related to the interannual and quasi-biennial modes of ENSO (Mo 2000). The Pacific decadal oscillation (PDO) was developed by Mantua et al. (1997) to represent decadal variability in the Pacific Ocean. The PDO essentially represents the North Pacific part of the interdecadal Pacific oscillation (IPO). A comparison of low-pass-filtered time series of PDO and IPO show a correlation of 0.83 (Henley et al. 2015). Henley et al. (2015) developed the tripole index (TPI) (NOAA/Physical Sciences Laboratory 2022b) that is highly correlated to the IPO (0.85–0.97), depending on the sea surface temperature dataset used and filtering method. The TPI uses sea surface temperatures from three areas of the Pacific (North Pacific, tropical Pacific in the ENSO region, and southwest South Pacific). An examination of the TPI compared to the IPO and PDO for cold events showed similar results, so only the TPI will be used in the following discussions.

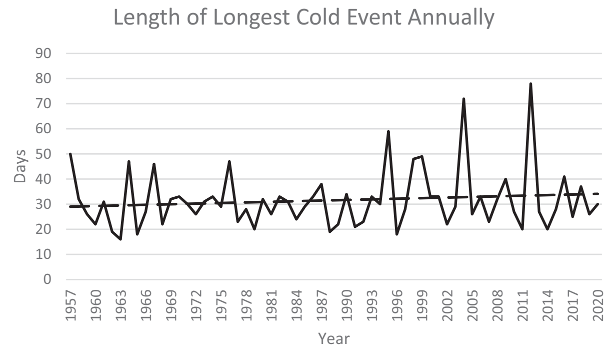

FIG. 1. Longest extreme cold event each year from 1957 to 2020. The dashed line is the trend over the period that is not statistically significant.

3. Results

a. Length and timing of cold events

The longest extreme cold period from each year between 1957 and 2020 is shown graphically in Fig. 1. An F test for variance comparing the first and second halves of the record shows that the increase in the variability of the longest event annually is not statistically significant. A t test on the long-term trend indicates it is not statistically significant. Table 1, which displays only events lasting longer than 40 days, emphasizes the anomalous length of recent extreme cold periods. Some years had multiple events of considerable length that are not represented on the longest event graph. Figures 2a and 2b display the number of events lasting 20–39 days, and 40+ days per year, respectively. Most of the events are in the

TABLE 1. Time period of event as well as maximum and minimum temperature for events lasting 40 or more days.

Year	Start	End	Days	Tmax (°C)	Tmin (°C)
1957	22 Aug	10 Oct	50	−49.7	−74.4
1964	13 Apr	28 May	47	−51.1	−72.2
1967	21 May	5 Jul	46	−50.9	−72.8
1976	26 Jun	10 Aug	47	−50.0	−76.0
1995	3 Aug	30 Sep	59	−50.1	−78.2
1998	9 Aug	25 Sep	48	−49.8	−76.7
1999	31 Mar	18 May	49	−49.9	−74.2
2004	21 Jun	31 Aug	72	−49.9	−77.7
2009	13 Jul	21 Aug	40	−50.5	−72.2
2012	5 Jul	20 Sep	78	−50.6	−76.0
2016	21 Jun	31 Jul	41	−50.5	−75.0

shorter ranges and are distributed over the entire period, but the longest (40+ days) occur only before 1977 or after 1994. To represent all events of considerable length and for comparison to Fig. 2, the number of event days per year was calculated by adding the length of all events lasting 20+ days for a given year and are presented in Fig. 3. The long-term trend is not statistically significant. The trends of the number of events occurring during the three Pacific circulation regimes that will be discussed in section 3e are also plotted in Fig. 3. Only the rising trend for the 1977–99 period is statistically significant at the 1% level. The increasing number of event days for this period would indicate that the mean temperature for the winter must be cooling. Figure 4 shows the frequency distribution of all the event days from 1957 to 2020 (encompassing 20+ day events) by month. Though cold events occurred from March to October, they were more common in the late winter season. This is as expected given the characterizations of the five seasons presented in Lazzara et al. (2012) with the temperature of the early winter (AMJ) at −57.74°C while the late winter (JAS) is −59.48°C.

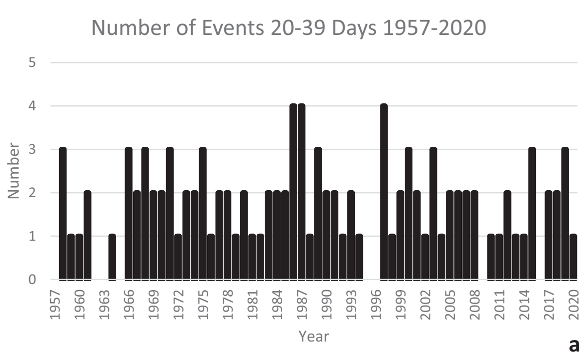

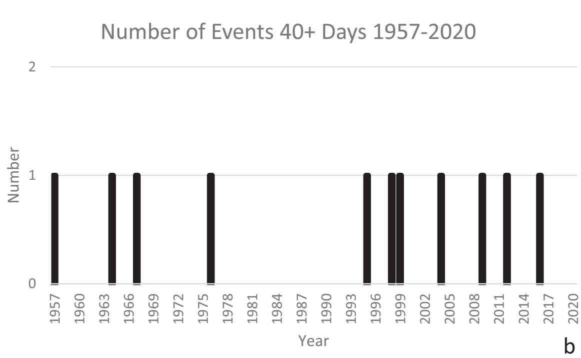

FIG. 2. (a) Number of events lasting 20–39 days from 1957 to 2020. (b) Number of events lasting 40 days or more.

While almost all of the cold events occur during early or late winter, the spring (ON) and autumn (FM) are more crucial to aircraft operations as cargo and passenger flights may still be occurring. The earliest a cold event has occurred in the autumn is 28 February 1961. Two events occurred in the 1960s and two in the 1980s. There have been no cold events starting in February through the middle of March since 1985. The latest ending of a cold event in the spring is 1 November 1997. Five events that started in September lasted into early to middle October, but only one of these occurred after 1986.

b. Station pressure and temperature averages

Average daily station pressure and maximum/minimum temperatures were calculated for each event of each year from 1957 to 2020. These values were compiled into averages for events lasting 20–39 days and 40+ days as well as seasonal averages. Events lasting 20–39 days averaged a maximum temperature of −58.95°C (±4.1°C), minimum of −66.20°C (±4.8°C), and pressure of 676.2 hPa (±25.5 hPa), while 40+ day events averaged −59.18°C (±1.8°C), −66.4°C (±1.8°C), and 674.7 hPa (±13.8 hPa), respectively. The values in parentheses represent two standard deviations from the mean. A closer look at the seasonal averages shows that the events with the coldest average maximum or minimum temperature and lowest average pressure occur in the late winter season. Additionally, the average pressure and maximum/minimum temperature values during the record-breaking event of 2012 were not out of the ordinary (674.4 hPa, −58.4°C, −65.8°C) in comparison to both the 20–39 day and 40+ day event average values. This suggests the similarity of all extreme cold events independent of length, which is consistent with the meteorological pattern associated with extreme cold periods, discussed below.

c. Changes in conditions during a cold event

Prolonged cold periods at the Pole are characterized by an initial decrease in pressure of around 15 hPa over 4 days, as well as a consistent set of wind shifts. The pressure rises and falls during an event due to passing synoptic-scale cyclones and mesoscale features (Neff et al. 2018). The location of the South Pole station in relation to the topography of the continent controls the direction of the wind shifts (Russell 1997; Neff 1999; Hogan and Gow 1993; Neff et al. 2018; Turner et al. 2021). The mean wind direction is from grid northeast around 40° (Clem et al. 2020; Neff 1999; Lazzara et al. 2012). Cold air draining off the Polar Plateau flows down the slope toward the station. This leads to grid northeast to easterly wind directions, slower wind speeds, and clear skies leading to colder

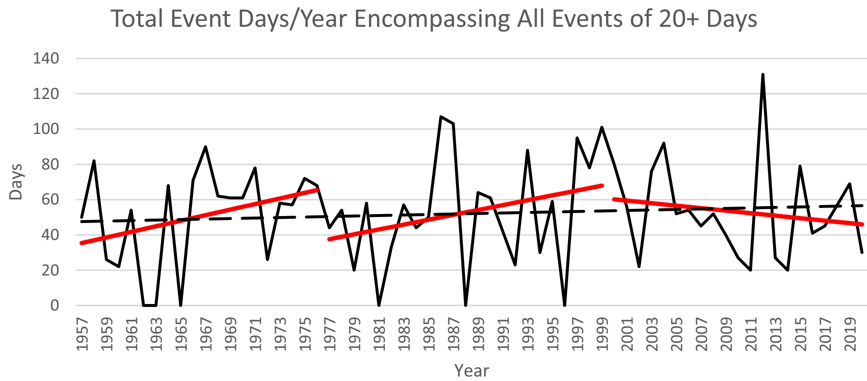

FIG. 3. Total event days per year for 1957–2020 (black line). First red line: trend for the total event days for 1957–76; second red line: trend for the total event days for 1977–99, significant at the 1% level; and third red line: trend for the total event days for 2000–20. The black dashed line shows the trend for the entire period, which is not statistically significant.

temperatures. Warm air, on the other hand, is advected inland over Coats Land and Queen Maud Land by synoptic-scale cyclones from the eastern Weddell Sea (Neff et al. 2018; Turner et al. 2021; Clem et al. 2020). This is reflected in the grid northwest switch in wind direction and a slight increase in wind speeds. (See Fig. 5 for geographical locations and direction of wind flow for cold and warm temperatures.) For most of the cases, wind speeds remained below 10 m s^{-1} for the entire event. In addition, an increase in clouds also helps increase the temperature due to the absorption and re-radiation of infrared radiation back to the surface.

d. The 2012 extreme event

The definition of a cold event implies persistent, cold temperatures below a specific threshold, and the event ends when temperatures rise above the threshold. An examination of daily cold event temperature maxima during the 2012 record event shows that the intensity of the cold event is reduced on an average of every 6–7 days by intrusions of warm air (Fig. 6) (Turner et al. 2021). These intrusions can raise the temperature by 10°–20° (over 1–6 days) without going above the −50°C threshold. The maximum temperature increase in an event was 26.7° over a 3-day period. The maximum increase to end an event was 29.7° over a 1-day period.

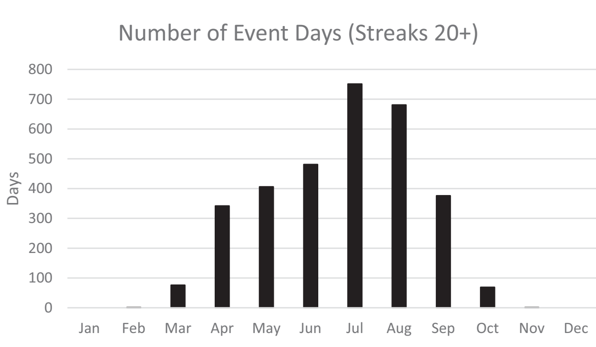

FIG. 4. Number of event days by month for 1957–2020.

Mean 600-hPa height composites for warm and cold temperature days were prepared from European Centre for Medium-Range Weather Forecasts Reanalysis version 5 (ERA5) data (Hersbach et al. 2020) to show the prevailing upper-level patterns. For a warm day (25 July), the mean heights show a trough over the Amundsen and Ross Seas and across the Antarctic Peninsula into the western Weddell Sea, with a broad height minimum over Enderby and Queen Maud Lands (Fig. 7) (Clem et al. 2020). As the air moves cyclonically around the trough in the Weddell Sea, warmer temperatures are advected over Queen Maud Land and Coats Land and into the South Pole region (Clem et al. 2020). Conditions at the Pole show winds out of grid north at 9.1 m s^{-1} with the temperature close to the cutoff marking the end of an event. For the next few days, the wind begins to change to grid northeast as the temperature falls below −60°C and the wind speeds drop to 5.5 m s^{-1}. Figure 8 shows the pattern on 31 July, where a height minimum is centered over the continent with troughs over the Ross Sea, the Bellingshausen Sea into the western Weddell Sea, into the South Atlantic, and Queen Maud Land. The rest of East Antarctica has another trough from Enderby Land to Wilkes Land (Neff et al. 2018). The geopotential height gradient is stronger on the Pacific side of the continent while the gradient has relaxed on the Atlantic side. As the cold settles in, the wind direction continues to move toward grid east as the wind speeds stay low. After several more days of cold, the cycle begins to repeat with the wind moving back to grid northeast and the speed increasing. The wind rose for the cold event (Fig. 9) shows the predominant wind direction as grid east with fewer occurrences from grid north to northeast similar to the divisions found by Neff (1999) and Clem et al. (2020). Using a chi-squared (χ^2) test, the distribution of wind direction and temperature is significant at the 5% level, and the distribution of wind speed and wind direction is significant at the 1% level. The mean wind speed for the grid north to northeast directions is 6.7 m s^{-1} and the grid northeast to east directions is 5.2 m s^{-1}.

Using the heights reported during the South Pole radiosonde ascent to measure the depth of the lower layers, the

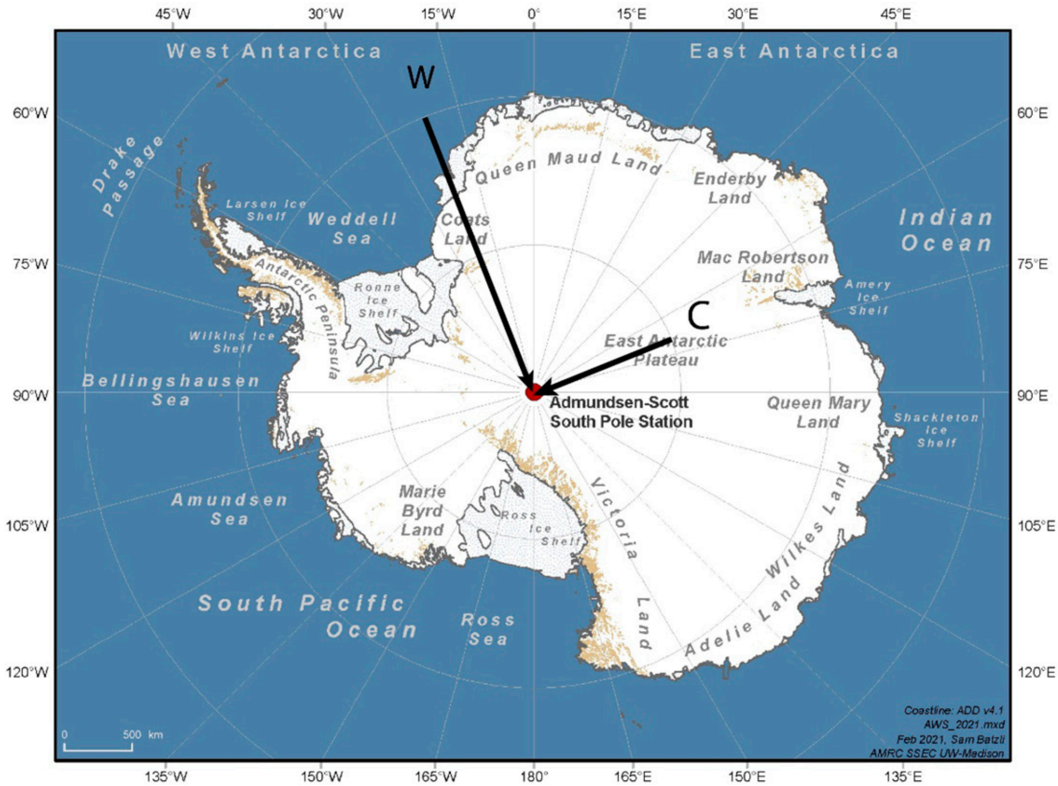

FIG. 5. Geographical map of Antarctica. Arrows show the direction of air flowing to the South Pole for warm days (W) and cold days (C).

state of the lower boundary layer illustrates the differences between warm and cold airflow. For 25 July, an isothermal lowest layer of about 30 m is topped by an inversion that reaches up to 600 hPa, indicating that the warm airflow is a very shallow (Fig. 10a). The decrease in temperature by 31 July shows an inversion at the surface of about 20°C reaching to a height of about 200 m where the temperature turns more isothermal (Fig. 10b). The warm periods are accompanied by an increase in clouds, a relationship that is statistically significant at the 0.1% level (Fig. 11a). The relationship between wind speed and temperature is also positively correlated and statistically significant at the 1% level (Fig. 11b).

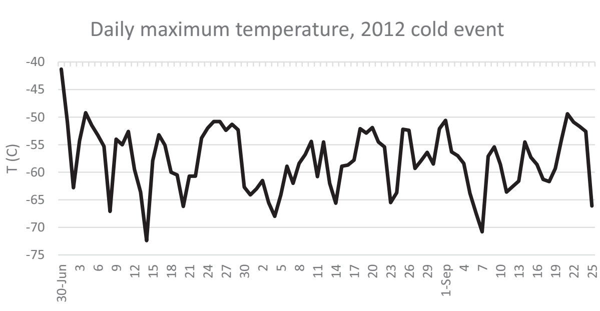

FIG. 6. Daily maximum temperatures for 30 Jun–25 Sep 2012. The cold event lasted from 5 Jul to 20 Sep.

e. Teleconnection indices during cold events

The long time series of temperature at the South Pole reflects multiple weather regimes over the period studied from decadal changes represented by the TPI and SAM to the 2–4-yr periods of ENSO. These overlapping influences can initiate large circulation pattern changes if they are coincident or, if the signals interfere, a neutral effect can result. Three Pacific circulation regimes have been identified using the TPI (Henley et al. 2015; NOAA/Physical Sciences Laboratory 2022b): a cool regime from 1945 to 1976, a warm regime from 1977 to 1999, and then back to a cool regime from 2000 to 2020. The warm regime (+TPI) is characterized by cold North Pacific sea surface temperatures (SST), warm SSTs in the tropical eastern Pacific, and cool SSTs in the southwest Pacific with a warm area in the Amundsen Sea. The cool regime (−TPI) has warm SSTs in the North Pacific, cool SSTs in the tropics, warm SSTs off the coast of Australia, and cool SSTs along the Pacific coast of Antarctica. The 1976–77 circulation change in the Pacific from cool to warm has been well documented (Miller et al. 1994; Hartmann and Wendler 2005; Wu et al. 2005; Mantua et al. 1997).

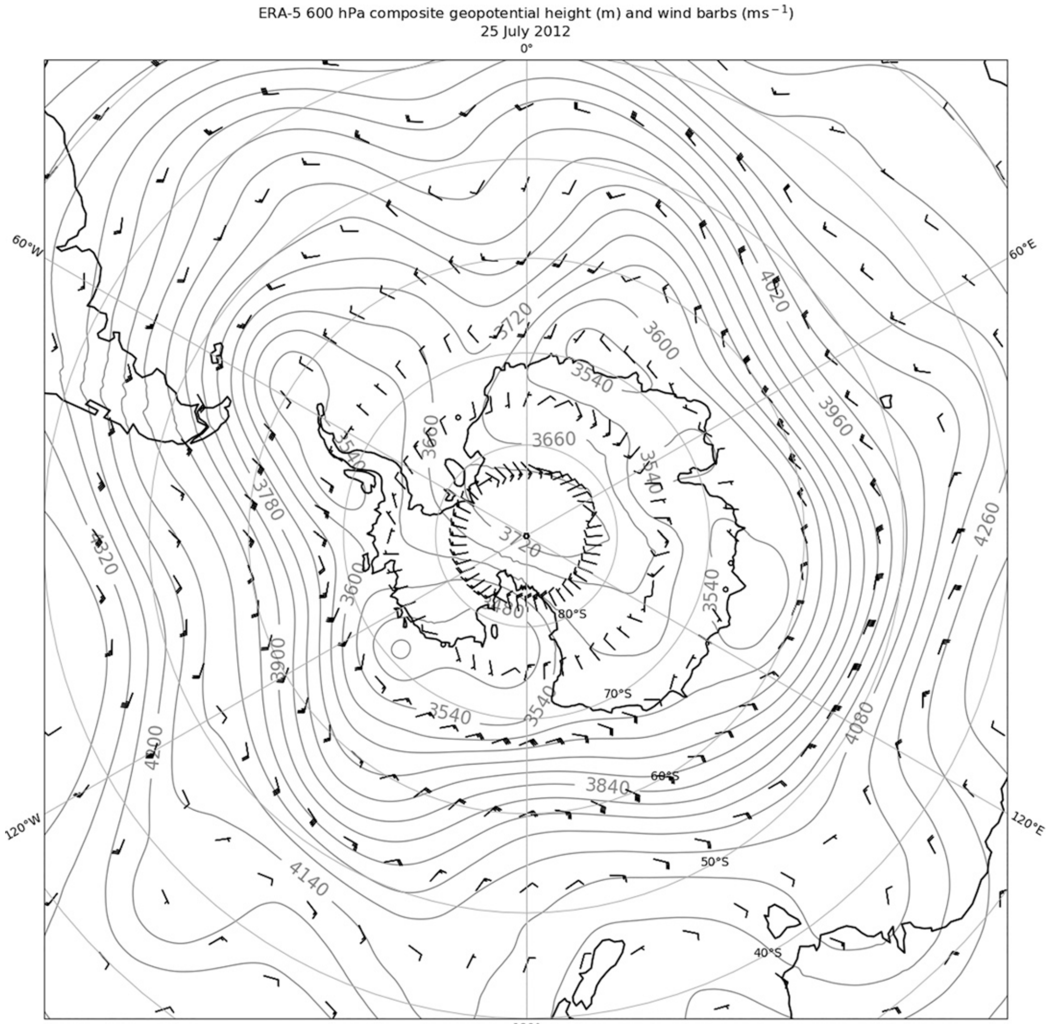

FIG. 7. Composite mean of 600-hPa geopotential heights for a warm day during the 2012 event (25 Jul).

The cold events were categorized by the phase of the TPI (warm, cool, or neutral) and the length of the cold event. The warm and cool phases of the TPI were determined as occurring more/less than ±0.4 for the TPI for the 1957–2020 period, respectively. These limits are based on the lowest one-third of the IPO/TPI values, following Clem et al. (2020). Anything in between was labeled neutral. The number of events for the different combinations of TPI and SAM were examined. While the most events occurred with −TPI and +SAM, this was not a statistically significant relationship.

On a hemispheric basis, the SAM index (Marshall 2003, 2022; Marshall et al. 2013) represents the condition of the polar vortex. A strong, symmetrical vortex (+SAM) is an indication of strong westerlies over the Southern Ocean, and a cold pattern at the South Pole (Thompson and Solomon 2002; Rogers and van Loon 1982; van den Broeke 1998b; Yuan and Li 2008). Planetary wave activity is more common when SAM is negative (−SAM) (Irving and Simmonds 2015). A comparison of the SAM indices during months containing cold events showed that almost half of the cold events occurred when SAM was positive (Table 2). However, 8 out of 11 of the longest events (40+ days) occurred with +SAM. For the record event in 2012, the SAM index was large and positive at the beginning of the event but decreased to neutral by the end of the event.

The absence of events lasting over 40 days (Fig. 2b) occurred at about the same time as the change in the Pacific circulation from a cool to a warm regime (1976–77) (Mantua et al. 1997). Events lasting from 20 to 39 days stayed at approximately the same level of activity. Examining total winter days below −50°C by year for early winter (see Fig. 12), shows a nearly neutral trend, which is not statistically significant. However, looking at the shorter time series based on the Pacific regimes, the 1957–76 segment trend is not statistically significant, but the rapid increase during the 1977–99 period that also began during the regime change was statistically significant at the 1% level. This rapid increase in the number of

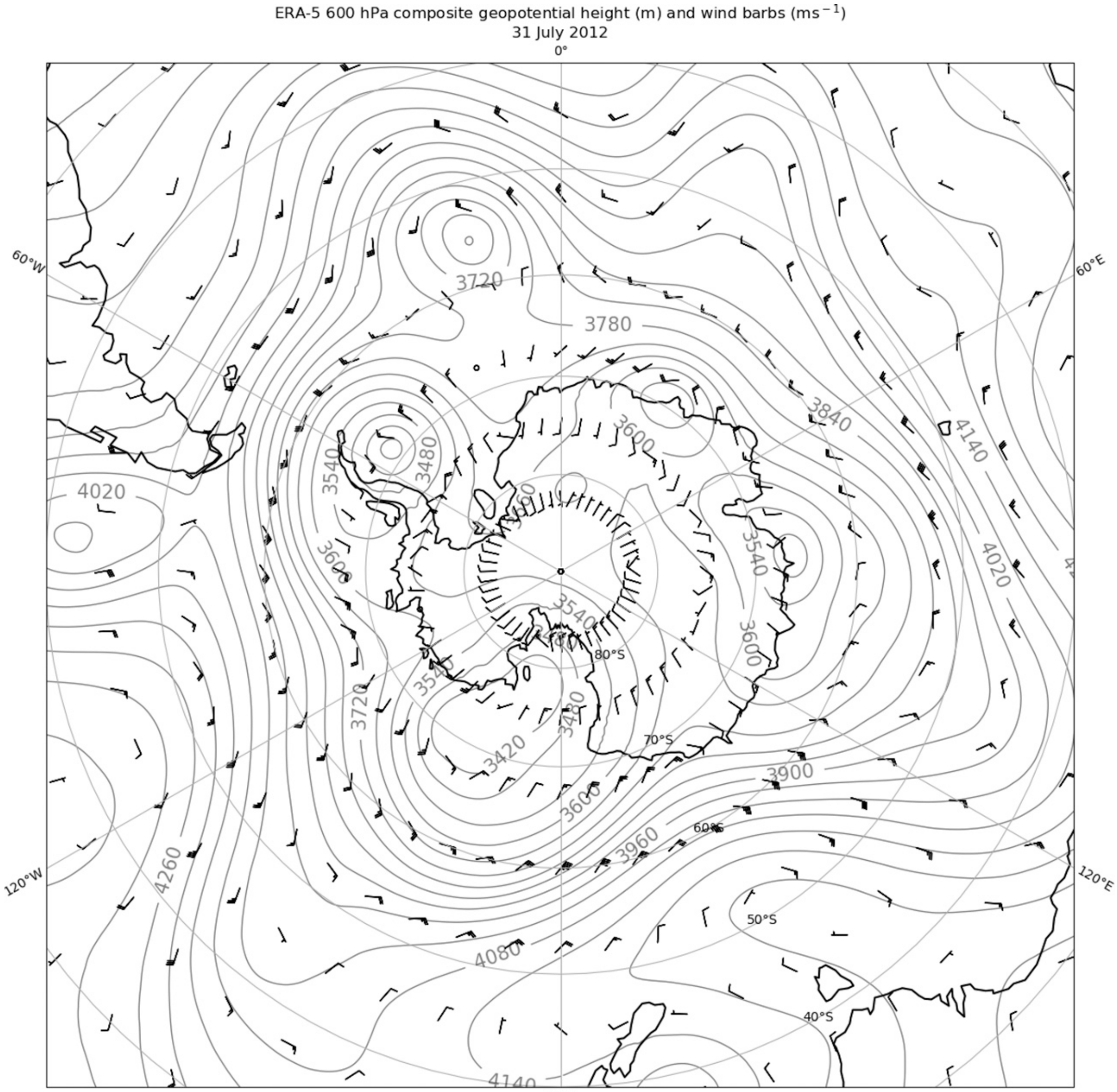

FIG. 8. Composite mean of 600 hPa geopotential heights for a cold day during the 2012 event (31 Jul).

days below −50°C is indicative of a cooling trend in the early winter for this time period. The rapid decrease that followed as the Pacific regime changed once again for the 2000–20 period was statistically significant at the 5% level. The switch in trend now shows that the latest 20 years have been a time of rapid warming in the early winter. The long-term late winter trend is not statistically significant (Fig. 13). Each of the shorter-term trends show a slow, continual rise of the number of winter days below −50°C, but none of the trends is statistically significant. The shorter-term trends point to less warming in the late winter, even though the annual trend in temperature shows an increase.

On shorter time scales, the presence or absence of an ENSO event and the position of the sea surface temperature (SST) anomaly (eastern or central Pacific) can also alter the prevailing circulation pattern in the Pacific. The positive phase of the PSA pattern has a negative pressure anomaly southeast of Australia, a positive pressure anomaly in the Amundsen–Bellingshausen Sea region, and a negative pressure anomaly in the Weddell Sea. This pattern is conducive to warm air advection over Queen Maud Land and into the South Pole region (Irving and Simmonds 2016; Clem et al. 2020). The connection between SAM and ENSO has been explored by Fogt et al. (2012) and Fogt and Marshall (2020).

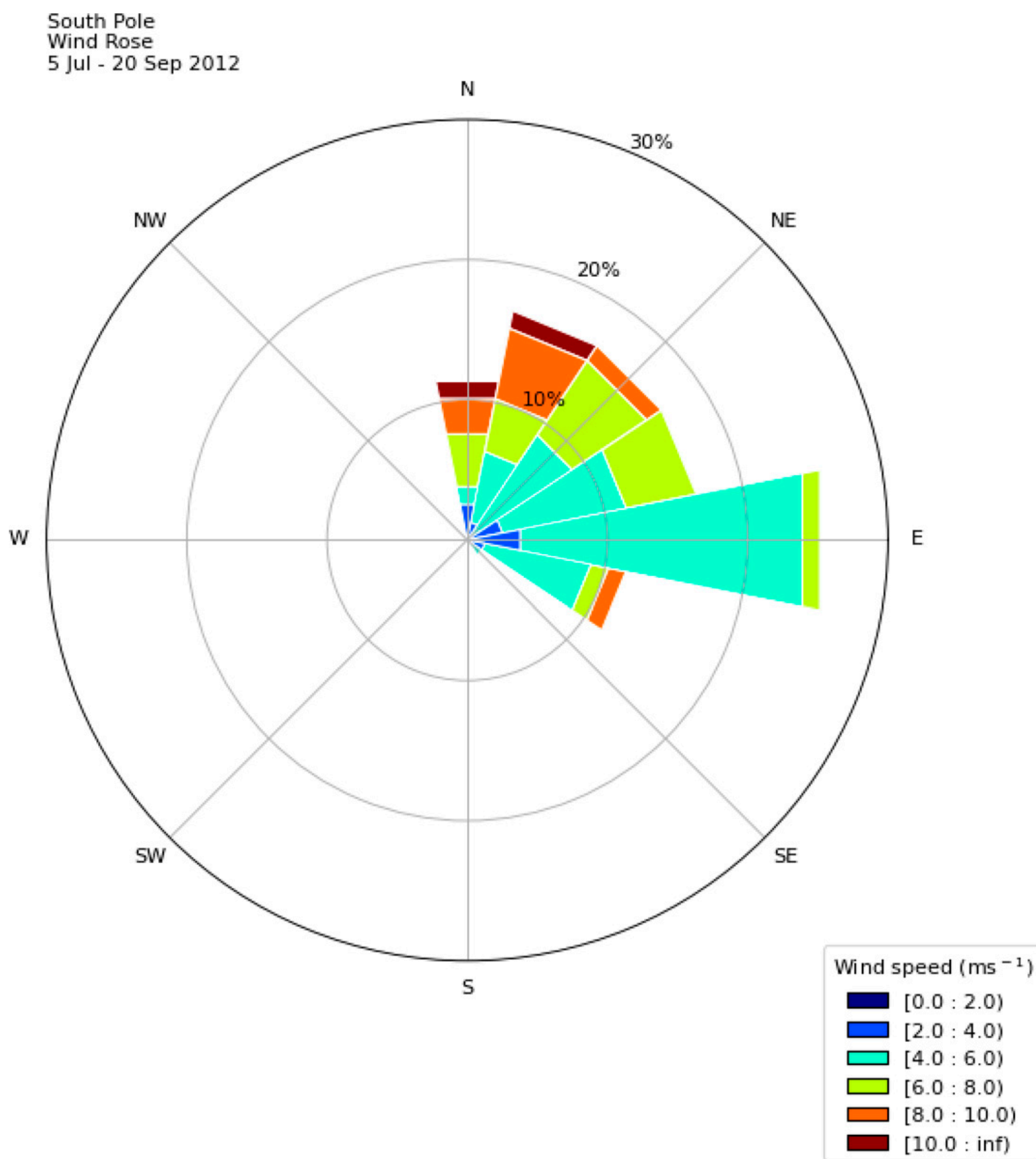

FIG. 9. Wind rose showing wind directions for the 2012 cold event. Grid north and northeast directions reflect the warm air intrusions, while the grid east direction shows the predominance of cold air into the region. Wind speeds are in m s^{-1}.

The strongest teleconnection occurs with La Niña/+SAM or El Niño/−SAM. For the cold events almost half (56) occurred during neutral conditions while 36 were during El Niño and 29 were during La Niña. In addition, half of the ENSO events were in the central Pacific (61) and almost half were in the eastern Pacific (56). A total of 18 of the central Pacific ENSO events were La Niña and 26 of the eastern Pacific events were El Niño. The most active time for eastern Pacific El Niño events during cold events was the warm regime of 1977–99 which is also when 6 cold events of 30 days or longer occurred, the largest number for any of the Pacific regimes. The most active time for central Pacific La Niña events during cold events was the cold regime of 1957–76. None of the relationships between events and SAM and ENSO teleconnections is statistically significant.

4. Discussion and conclusions

As noted at the beginning of this study, the state of warm or cold advection into the South Pole region is controlled by the position and strength of the polar vortex as well as the location of pressure anomalies near the Weddell Sea. In turn, those pressure anomalies are related to the position and strength of the Amundsen Sea low (ASL). The strength and

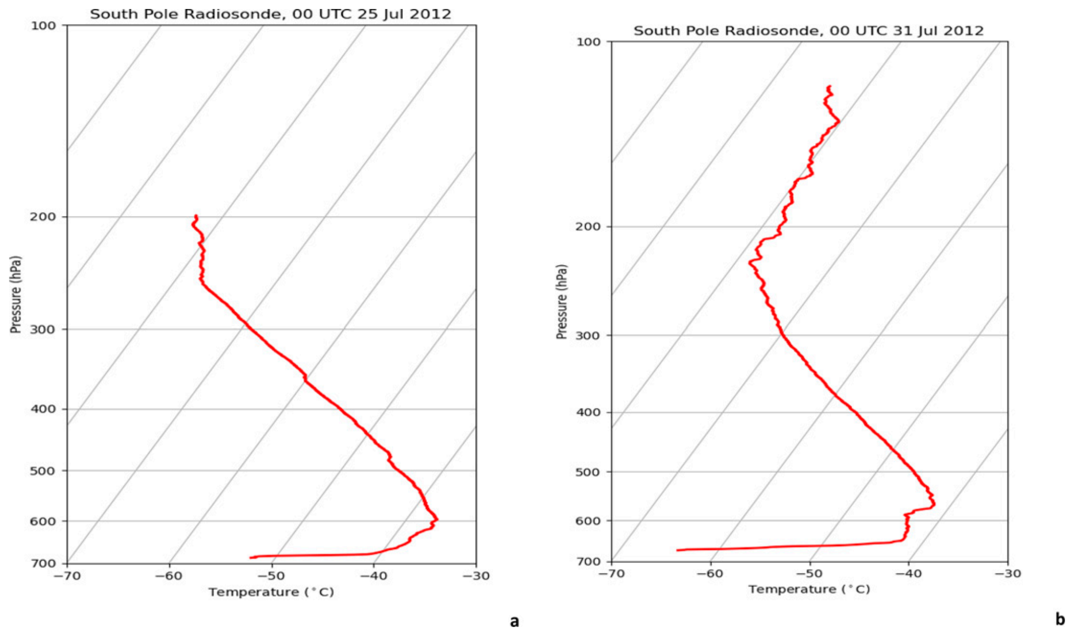

FIG. 10. (a) Radiosonde sounding for 25 Jul 2012 showing the smaller inversion above an isothermal layer of about 30 m for warm temperatures during a cold event. (b) Radiosonde sounding for 31 Jul 2012 showing the strong inversion typical of the colder temperatures during the cold events.

position of the ASL respond to many different factors. Seasonally, the ASL moves west and south during the winter and east and north during the summer (Turner et al. 2013; Fogt et al. 2012). ENSO has a variety of effects including a deeper ASL with La Niña (Clem et al. 2018; Fogt et al. 2011), and a farther east position with an eastern Pacific El Niño (Wilson et al. 2014). For the hemispheric-scale indices, the ASL has higher pressure with −SAM (Turner et al. 2013), and a lower pressure with +SAM (Fogt et al. 2011), and the combination of −TPI/+SAM moves the ASL to the western Weddell Sea (Clem et al. 2020).

Clem et al. (2020) reported on the annual warming at the South Pole over a 30-yr period (1989–2018); see also Stammerjohn and Scambos (2020). In this study, an examination of the mean monthly maximum and minimum temperatures for that period indicates that the extremes of each month were warming, but July was cooling (not shown). The strongest warming occurred in May and October (greater than 1°C decade^{-1}) for both mean maximum and minimum temperatures. At the same time, the number of days below −50°C in early winter has been decreasing since 1999 (Fig. 12) which is significant at the 5% level. The warming that is occurring during early winter (AMJ) corroborates with the autumn pattern (MAM) of intense flow from the Weddell Sea and increase in temperature show in Clem et al. (2020), (extended data, Fig. 6). Late winter shows an increase in the number of days below −50°C for the same period (Fig. 13) which is not statistically significant. Most of the cold events that are 40 days or longer have occurred since 1994 and are almost evenly divided between early and late winter.

The lack of statistical significance for any relationship of the cold events with the large-scale processes makes it difficult to identify specific causes or signals that a cold event is about to commence. Summarizing the results of all the various factors discussed above gives an indication of what would be needed to trigger a cold event. For a cold period, a strong polar vortex is centered approximately over the South Pole. In general, this would be reflected as a +SAM situation with strong westerly winds over the Southern Ocean, a deep ASL and increased heights over the continent. A La Niña episode would favor lower pressure in the Amundsen Sea region, and a central Pacific ENSO would trigger a PSA pattern that forms in a more westerly position than the eastern Pacific ENSO. In addition, more events occur with +SAM in a warm regime, and +TPI in a warm regime or −TPI in a cool

TABLE 2. Number of cold events occurring during Pacific warm and cold regimes for SAM and ENSO.

	SAM			ENSO		
Years and regime	Positive	Neutral	Negative	El Niño	Neutral	La Niña
1957–76 cold	13	8	15	10	14	12
1977–99 warm	21	12	13	18	18	10
2000–20 cold	18	13	8	8	24	7
All years	52	33	36	36	56	29

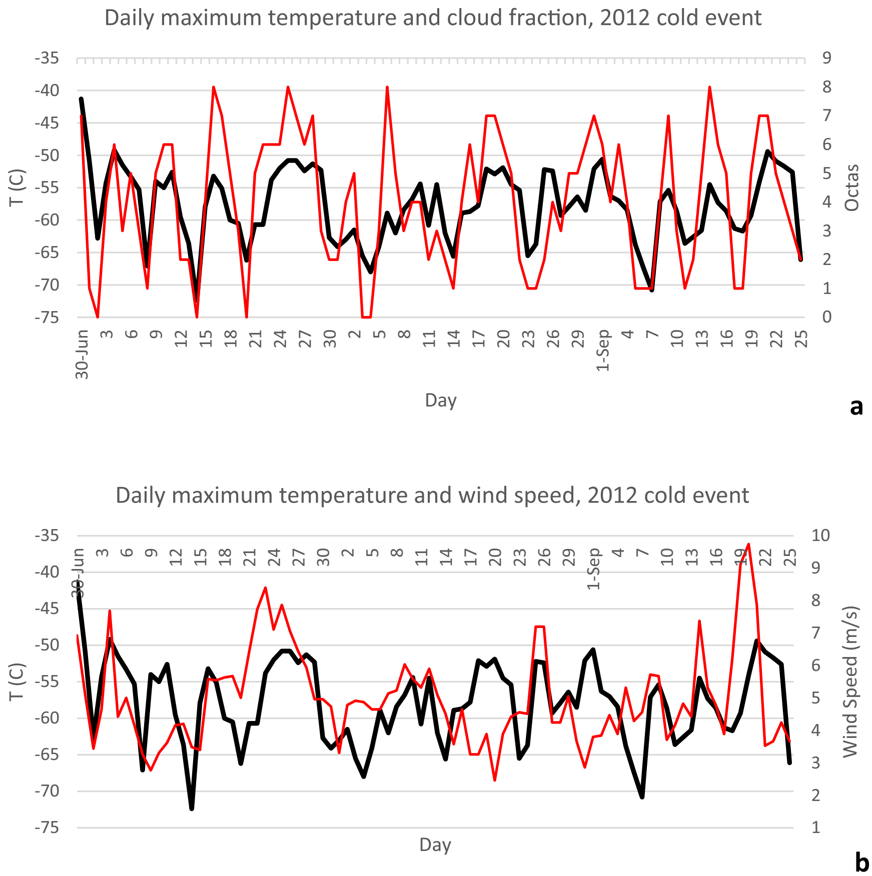

FIG. 11. Daily maximum temperatures for 30 Jun–25 Sep 2012. The cold event lasted from 5 Jul to 11 Sep. (a) Temperature (black line) and cloud fraction (red line) are significantly correlated at the 0.1% level. (b) Temperature (black line) and wind speed (red line) are significantly correlated at the 1% level.

regime. The intrusion of warm air from the Weddell Sea every 6–7 days occurs when a cyclone is centered over the western Weddell Sea and a ridge is centered over the eastern Weddell Sea and into Queen Maud Land (Neff 1999; Neff et al. 2018; Clem et al. 2020). This cycle would indicate that there are other additional mechanisms on the synoptic scale that affect the temperature at the South Pole. Mesoscale eddies, internal variability, and topography also contribute to the cycle of temperatures in a very complex region (O'Kane et al. 2017; Neff et al. 2018).

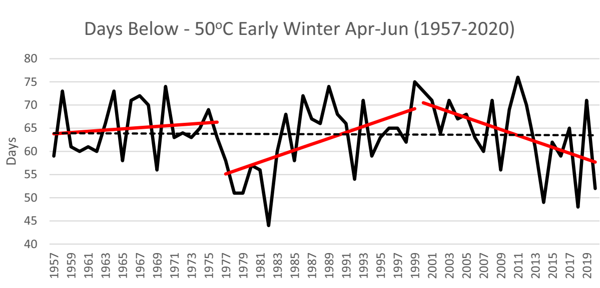

FIG. 12. Total number of days below −50°C from 1957 to 2020 for early winter (April–June). First red line: trend for the total number of days below −50°C from 1957 to 1976; second red line: trend for the total number of days below −50°C from 1977 to 1999, which is significant at the 1% level; and third red line: trend for the total number of days below −50°C from 2000 to 2020, which is significant at the 5% level. The dashed line is the trend for the entire period, which is not statistically significant.

Based on the warming temperatures found by Clem et al. (2020) and this study for early winter, it might be expected that lengthy cold events would not be occurring with regular frequency. The late winter has some cooling during July, but this is not statistically significant. However, the state of the Pacific Ocean circulation also should be considered. The Southern Hemisphere has been in a cool regime since 2000 with TPI negative or neutral and +SAM, and the tropical SSTs were cooling into a weak La Niña pattern by mid-2021. The +SAM/−TPI combination has been associated with a higher number of cold events occurring even though that relationship is not statistically significant. If the Pacific circulation would switch to a warm regime or SAM would move to neutral or negative, the number of cold events might drop even further. These results have implications for flight operations to Amundsen–Scott South Pole station. A reduction in these

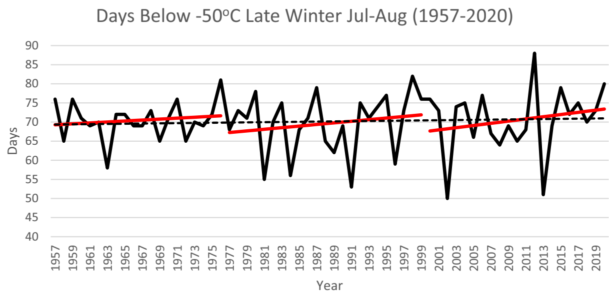

FIG. 13. Total number of days below −50°C from 1957 to 2020 for late winter (July–September). First red line: trend for total number of days below −50°C from 1957 to 1976; second red line: trend for the total number of days below −50°C from 1977 to 1999; and third red line: trend for the total number of days below −50°C from 2000 to 2020. Dashed line is the trend for the entire period. None of the trends are statistically significant.

events may allow greater aviation access to the station. The large-scale dynamical forcings that affect the occurrence of these events will dictate access to the station by aircraft.

Acknowledgments. This material as well as the AWS data are based upon work supported by the National Science Foundation under 1141908, 1245663, 1543305, and 1924730. The authors appreciate the comments and suggestions from Dr. William Neff and two anonymous reviewers that made this a better report. Special thanks to Dr. Jonathan Martin for his comments and to Dr. Sam Batzli for the Antarctic map. Additional thanks go to Elena Sarasino and Carol Costanza for their assistance.

Data availability statement. South Pole data used in this study are openly available from the Antarctic Meteorological Research Center at https://amrc.ssec.wisc.edu/usap/southpole/. The SAM datasets are openly available from the British Antarctic Survey (http://www.nerc-bas.ac.uk/icd/gjma/sam.html). The ONI is openly available from the National Weather Service Climate Prediction Center (https://origin.cpc.ncep.noaa.gov/products/analysis_monitoring/ensostuff/ONI_v5.php). The SST anomalies in the Niño-3 and Niño-4 areas are openly available from the Physical Sciences Laboratory of the National Oceanic and Atmospheric Administration (NOAA) (https://psl.noaa.gov/gcos_wgsp/Timeseries/Nino3/; https://psl.noaa.gov/gcos_wgsp/Timeseries/Nino4/). The TPI is openly available from NOAA (https://psl.noaa.gov/data/timeseries/IPOTPI/).

ERA5 data are freely available from ECMWF (https://cds.climate.copernicus.eu/#!/search?text=ERA5&type=dataset).

REFERENCES

Ashok, K., S. K. Behera, S. A. Rao, H. Weng, and T. Yamagata, 2007: El Niño Modoki and its possible teleconnection. *J. Geophys. Res.*, **112**, C11007, https://doi.org/10.1029/2006JC003798.

——, C.-Y. Tam, and W.-J. Lee, 2009: ENSO Modoki impact on the Southern Hemisphere storm track activity during extended austral winter. *Geophys. Res. Lett.*, **36**, L12705, https://doi.org/10.1029/2009GL038847.

Clem, K. R., J. A. Renwick, and J. McGregor, 2018: Autumn cooling of western East Antarctica linked to the tropical Pacific. *J. Geophys. Res. Atmos.*, **123**, 89–107, https://doi.org/10.1002/2017JD027435.

——, R. L. Fogt, J. Turner, B. R. Lintner, G. J. Marshall, J. R. Miller, and J. A. Renwick, 2020: Record warming at the South Pole during the past three decades. *Nat. Climate Change*, **10**, 762–770, https://doi.org/10.1038/s41558-020-0815-z.

Connolley, W. M., 1996: The Antarctic temperature inversion. *Int. J. Climatol.*, **16**, 1333–1342, https://doi.org/10.1002/(SICI)1097-0088(199612)16:12<1333::AID-JOC96>3.0.CO;2-6.

Fogt, R. L., and G. J. Marshall, 2020: The Southern Annual Mode: Variability, trends, and climate impacts across the Southern Hemisphere. *Wiley Interdiscip. Rev.: Climate Change*, **11**, e652, https://doi.org/10.1002/wcc.652.

——, D. H. Bromwich, and K. M. Hines, 2011: Understanding the SAM influence on the South Pacific ENSO teleconnection. *Climate Dyn.*, **36**, 1555–1576, https://doi.org/10.1007/s00382-010-0905-0.

——, A. J. Wovrosh, R. A. Langen, and I. Simmonds, 2012: The characteristic variability and connection to the underlying synoptic activity of the Amundsen–Bellingshausen Seas low. *J. Geophys. Res.*, **117**, D07111, https://doi.org/10.1029/2011JD017337.

Hartmann, B., and G. Wendler, 2005: The significance of the 1976 Pacific climate shift in the climatology of Alaska. *J. Climate*, **18**, 4824–4839, https://doi.org/10.1175/JCLI3532.1.

Henley, B. J., J. Gergis, D. J. Karoly, S. B. Power, J. Kennedy, and C. K. Folland, 2015; A tripole index for the interdecadal Pacific Oscillation. *Climate Dyn.*, **45**, 3077–3090, https://doi.org/10.1007/s00382-015-2525-1.

Hersbach, H., and Coauthors, 2020: The ERA5 global reanalysis. *Quart. J. Roy. Meteor. Soc.*, **146**, 1999–2049, https://doi.org/10.1002/qj.3803.

Hogan, A. W., and A. J. Gow, 1993: Particle transport to the snow surface at the South Pole: The beginning of a tropospheric history. *Tellus*, **45B**, 188–207, https://doi.org/10.3402/tellusb.v45i2.15592.

Huang, B., and Coauthors, 2017: Extended Reconstructed Sea Surface Temperature, version 5 (ERSSTv5): Upgrades, validations, and intercomparisons. *J. Climate*, **30**, 8179–8205, https://doi.org/10.1175/JCLI-D-16-0836.1.

Irving, D., and I. Simmonds, 2015: A novel approach to diagnosing Southern Hemisphere planetary wave activity and its influence on regional climate variability. *J. Climate*, **28**, 9041–9057, https://doi.org/10.1175/JCLI-D-15-0287.1.

——, and ——, 2016: A new method for identifying the Pacific–South American pattern and its influence on regional climate variability. *J. Climate*, **29**, 6109–6125, https://doi.org/10.1175/JCLI-D-15-0843.1.

Keller, L. M., K. A. Baker, M. A. Lazzara, and J. Gallagher, 2009: A comparison of meteorological observations from South Pole station before and after installation of a new instrument suite. *J. Atmos. Oceanic Technol.*, **26**, 1605–1613, https://doi.org/10.1175/2009JTECHA1220.1.

Lachlan-Cope, T., and W. Connolley, 2006: Teleconnections between the tropical Pacific and the Amundsen-Bellingshausen Sea: Role of the El Niño/Southern Oscillation. *J. Geophys. Res.*, **111**, D23101, https://doi.org/10.1029/2005JD006386.

Lazzara, M. A., L. M. Keller, T. Markle, and J. Gallagher, 2012: Fifty-year Amundsen-Scott South Pole station surface climatology. *Atmos. Res.*, **118**, 240–259, https://doi.org/10.1016/j.atmosres.2012.06.027.

Mantua, N. J., S. R. Hare, Y. Zhang, J. M. Wallace, and R. C. Francis, 1997: A Pacific interdecadal climate oscillation with impacts on salmon production. *Bull. Amer. Meteor. Soc.*, **78**, 1069–1079, https://doi.org/10.1175/1520-0477(1997)078<1069:APICOW>2.0.CO;2.

Marshall, G. J., 2003: Trends in the southern annular mode from observations and reanalyses. *J. Climate*, **16**, 4134–4143, https://doi.org/10.1175/1520-0442(2003)016<4134:TITSAM>2.0.CO;2.

——, A. Orr, and J. Turner, 2013: A predominant reversal in the relationship between the SAM and East Antarctic temperatures during the twenty-first century. *J. Climate*, **26**, 5196–5204, https://doi.org/10.1175/JCLI-D-12-00671.1.

——, 2022: An observation-based Southern Hemisphere Annular Mode Index. British Antarctic Survey, Natural Environment Reseach Council, accessed 5 January 2021, http://www.nerc-bas.ac.uk/icd/gjma/sam.html.

McCormick, R. A., 1958: An estimate of the minimum possible surface temperature at the South Pole. *Mon. Wea. Rev.*, **86**, 1–5, https://doi.org/10.1175/1520-0493(1958)086<0001:AEOTMP>2.0.CO;2.

Miller, A. J., D. R. Cayan, T. P. Barnett, N. E. Graham, and J. M. Oberhuber, 1994: The 1976–77 climate shift of the Pacific Ocean. *Oceanography*, **7**, 21–26, https://doi.org/10.5670/oceanog.1994.11.

Mo, K., 2000: Relationships between low-frequency variability in the Southern Hemisphere and sea surface temperature anomalies. *J. Climate*, **13**, 3599–3610, https://doi.org/10.1175/1520-0442(2000)013<3599:RBLFVI>2.0.CO;2.

Monaghan, A. J., D. H. Bromwich, H.-L. Wei, A. M. Cayette, J. G. Powers, Y.-H. Kuo, and M. A. Lazzara, 2003: Performance of weather forecast models in the rescue of Dr. Ronald Shemenski from the South Pole in April 2001. *Wea. Forecasting*, **18**, 142–160, https://doi.org/10.1175/1520-0434(2003)018<0142:POWFMI>2.0.CO;2.

Neff, W. D., 1999: Decadal time scale trends and variability in the tropospheric circulation over South Pole. *J. Geophys. Res.*, **104**, 27 217–27 251, https://doi.org/10.1029/1999JD900483.

——, J. Crawford, M. Buhr, J. Nicovich, G. Chen, and D. Davis, 2018: The meteorology and chemistry of high nitrogen oxide concentrations in the stable boundary layer at the South Pole. *Atmos. Chem. Phys.*, **18**, 3755–3778, https://doi.org/10.5194/acp-18-3755-2018.

NOAA/NWS/Climate Prediction Center, 2022: Cold & warm episodes by season. NOAA/NWS/CPC, accessed 5 January 2021, https://origin.cpc.ncep.noaa.gov/products/analysis_monitoring/ensostuff/ONI_v5.php.

NOAA/Physical Sciences Laboratory, 2022a: GCOS-AOPC/OOPC Working Group in surface pressure. NOAA/PSL, accessed 20 October 2020, https://psl.noaa.gov/gcos_wgsp/Timeseries/.

——, 2022b: TPI (IPO) tripole index for the interdecadal Pacific oscillation: Climate time series. NOAA/PSL, accessed 25 August 2021, https://psl.noaa.gov/data/timeseries/IPOTPI/.

O'Kane, T. J., D. P. Monselesan, and J. S. Risbey, 2017: A multiscale reexamination of the Pacific–South American pattern. *Mon. Wea. Rev.*, **145**, 379–402, https://doi.org/10.1175/MWR-D-16-0291.1.

Rayner, N. A., D. E. Parker, E. B. Horton, C. K. Folland, L. V. Alexander, D. P. Rowell, E. C. Kent, and A. Kaplan, 2003: Global analyses of sea surface temperature, sea ice, and night marine air temperature since the late nineteenth century. *J. Geophys. Res.*, **108**, 4407, https://doi.org/10.1029/2002JD002670.

Rogers, J. C., and H. van Loon, 1982: Spatial variability of sea level pressure and 500 mb height anomalies over the Southern Hemisphere. *Mon. Wea. Rev.*, **110**, 1375–1392, https://doi.org/10.1175/1520-0493(1982)110<1375:SVOSLP>2.0.CO;2.

Russell, C. A., 1997: A study of temperature anomalies at the South Pole and associated synoptic scale processes over Antarctica. M.A. thesis, Dept. of Geography, University of Colorado Boulder, 99 pp.

Siple, P. A., 1957: We are living at the South Pole. *Natl. Geogr. Mag.*, **112**, 5–35.

——, 1959: *90° South.* G. P. Putnam's Sons, 384 pp.

Stammerjohn, S. E., and T. A. Scambos, 2020: Warming reaches the South Pole. *Nat. Climate Change*, **10**, 710–711, https://doi.org/10.1038/s41558-020-0827-8.

Thompson, D. W. J., and S. Solomon, 2002: Interpretation of recent Southern Hemisphere climate change. *Science*, **296**, 895–899, https://doi.org/10.1126/science.1069270.

Turner, J., T. Phillips, J. S. Hosking, G. J. Marshall, and A. Orr, 2013: The Amundsen Sea low. *Int. J. Climate*, **33**, 1818–1829, https://doi.org/10.1002/joc.3558.

——, H. Lu, J. King, G. J. Marshall, T. Phillips, D. Bannister, and S. Colwell, 2021: Extreme temperatures in the Antarctic. *J. Climate*, **34**, 2653–2668, https://doi.org/10.1175/JCLI-D-20-0538.1.

van den Broeke, M. R., 1998a: The semi-annual oscillation and Antarctic climate. Part 1: Influence on near surface temperatures (1957–1979). *Ant. Sci.*, **10**, 175–183, https://doi.org/10.1017/S0954102098000248.

——, 1998b: The semi-annual oscillation and Antarctic climate. Part 2: Recent changes. *Ant. Sci.*, **10**, 184–191, https://doi.org/10.1017/S095410209800025X.

van Loon, H., 1967: The half-yearly oscillations in the middle and high southern latitudes and the coreless winter. *J. Atmos. Sci.*, **24**, 472–486, https://doi.org/10.1175/1520-0469(1967)024<0472:THYOIM>2.0.CO;2.

Wendler, G., and Y. Kodama, 1993: The kernlose winter in Adélie Coast. *Antarctic Meteorology and Climatology: Studies Based on Automatic Weather Stations*, D. H. Bromwich and C. R. Stearns, Eds., Antarctic Research Series, No. 61, Amer. Geophys. Union, 139–147.

Wilson, A. B., D. H. Bromwich, K. M. Hines, and S.-H. Wang, 2014: El Niño flavors and their simulated impacts on atmospheric circulation in the high southern latitudes. *J. Climate*, **27**, 8934–8955, https://doi.org/10.1175/JCLI-D-14-00296.1.

Wu, L., D. E. Lee, and Z. Liu, 2005: The 1976/77 North Pacific climate regime shift: The role of subtropical ocean adjustment and coupled ocean–atmosphere feedbacks. *J. Climate*, **18**, 5125–5140, https://doi.org/10.1175/JCLI3583.1.

Yuan, X., and C. Li, 2008: Climate modes in southern high latitudes and their impacts on Antarctic sea ice. *J. Geophys. Res.*, **113**, C06S91, https://doi.org/10.1029/2006JC004067.